Static and Dynamic Effects on Vicinal Scalar *J* Couplings in Proteins and Peptides: A MD/DFT Analysis

David A. Case,*,† Christoph Scheurer,‡,§ and Rafael Brüschweiler*,‡

Contribution from the Department of Molecular Biology, The Scripps Research Institute, La Jolla, California 92037, and Gustaf H. Carlson School of Chemistry and Biochemistry, Clark University, Worcester, Massachusetts 01610

Received May 23, 2000. Revised Manuscript Received August 15, 2000

Abstract: Vicinal scalar *J*-coupling constants in polypeptides are analyzed using density functional theory (DFT) in combination with molecular dynamics (MD) computer simulations. The couplings studied are the six ^3J-coupling constants that involve the φ backbone torsion angle, $^3J(H^N-H^\alpha)$, $^3J(H^N-C^\beta)$, $^3J(H^N-C')$, $^3J(C'-H^\alpha)$, $^3J(C'-C^\beta)$, and $^3J(C'-C')$, and two ^3J-coupling constants, $^3J(H^\alpha-N)$ and $^3J(N-N)$, that involve the ψ backbone torsion angle. The dependence of these couplings on their main torsion angle as well as other degrees of freedom are investigated by computations performed on two different versions of the alanine dipeptide, Ala-Ala-NH_2 and Ace-Ala-NMe, with sets of coordinates obtained by different structure optimization schemes and from snapshots extracted from a MD trajectory of ubiquitin. In this way, assumptions that underlie the widely used Karplus relationships can be independently tested. Static Karplus curves, which are fitted to the computed couplings as a function of the φ-torsion angle, are generally in good agreement with empirical Karplus curves reported for several proteins if substantial motional averaging effects are taken into account. For ubiquitin, the average φ-angle fluctuation amplitudes are $\pm 24°$, which is somewhat larger than what has been found from NMR relaxation measurements and MD simulations, presumably because these latter techniques predominantly reflect motions on the ns and sub-ns time-scale range. Systematic differences in the backbone φ angles between the solution-state and the crystalline structure are found to play a minor role. The two *J* couplings involving the ψ angle are sensitive not only to their main torsion angle, but also to other degrees of freedom, which may complicate their interpretation. The emergence of DFT as a quantitative tool for the interpretation of scalar *J*-coupling constants enhances the power of *J*-coupling analysis as a unique probe of structural dynamics of biomolecules.

1. Introduction

The potential of indirect spin−spin coupling constants for conformational analysis using NMR data has been recognized in the early days of liquid-state NMR. The establishment of a formal relationship by Karplus[1] between a vicinal scalar coupling constant of two spins and their intervening torsion angle stimulated a large number of methodological and applied work that continues today. In practice, Karplus relationships are empirically parametrized using *J*-coupling constants measured for systems with known structure, and are subsequently used to interpret couplings in systems with less well characterized or unknown structure.[2−4]

For peptides and proteins, backbone $^3J(H^N-H^\alpha)$ coupling constants have been measured extensively for the purpose of φ torsion angle characterization, and thereby to distinguish α-helical from β-sheet secondary structure. More recently, attention has turned to measurements of coupling constants involving ^{13}C or ^{15}N spins, providing independent information on φ, ψ, and χ_1 torsion angles.[5−15] Extensive measurements on two proteins, ubiquitin and flavodoxin, whose X-ray structures are known have lead to empirical calibrations of all six of the "Karplus curves" of ^3J couplings involving the φ backbone torsional angle.[6−8,16] These data provide a unique basis for comparison of measured and computed NMR parameters.

* Correspondence to be addressed to: Professor David A. Case, Department of Molecular Biology, The Scripps Research Institute, La Jolla, CA 92037. Telephone: (858) 784-9768. Fax: (858) 784-8896. E-Mail: case@scripps.edu. Professor Rafael Brüschweiler, Carlson School of Chemistry and Biochemistry. Clark University, Worcester, MA 01610-1477. Telephone: (508) 793-7220. Fax: (508) 793-8861. E-Mail: bruschweiler@nmr.clarku.edu.

† The Scripps Research Institute.

‡ Clark University.

§ Current address: Chemistry Department, University of Rochester, Rochester, NY. 14627-0216. E-mail: chris@feynman.chem.rochester.edu.

(1) Karplus, M. *J. Chem. Phys.* **1959**, *30*, 11−15. Karplus, M. *J. Am. Chem. Soc.* **1963**, *85*, 2870.

(2) Altona, C. In *Encyclopedia of Nuclear Magnetic Resonance*; Grant, D. M., Harris, R. K., Eds; Wiley: London, 1996.

(3) Bystrov, V. F. *Prog. Nucl. Magn. Reson. Spectrosc.* **1976**, *10*, 41−81.

(4) Case, D. A.; Dyson, H. J.; Wright, P. E. *Methods Enzymol.* **1994**, *239*, 392−416.

(5) Düx, P.; Whitehead, B.; Boelens, R.; Kaptein, R.; Vuister, G. W. *J. Biomol. NMR* **1997**, *10*, 301−306.

(6) Wang, A. C.; Bax, A. *J. Am. Chem. Soc.* **1996**, *118*, 2483−2494.

(7) Hu, J.-S.; Bax, A. *J. Am. Chem. Soc.* **1996**, *118*, 8170−8171.

(8) Hu, J.-S.; Bax, A. *J. Am. Chem. Soc.* **1997**, *119*, 6360−6368.

(9) Hu, J.-S.; Grzesiek, S.; Bax, A. *J. Am. Chem. Soc.* **1997**, *119*, 1803−1804.

(10) Löhr, F.; Blümel, M.; Schmidt, J. M.; Rüterjans, H. *J. Biomol. NMR* **1997**, *10*, 107−118.

(11) Löhr, F.; Rüterjans, H. *J. Am. Chem. Soc.* **1997**, *119*, 1468−1469.

(12) Schmidt, J. M. *J. Magn. Reson.* **1997**, *124*, 298−309.

(13) Pellcchia, M.; Fattorusso, R.; Wider, G. *J. Am. Chem. Soc.* **1998**, *120*, 6824−6825.

(14) Theis, K.; Dingley, A. J.; Hoffmann, A.; Omichinski, J. G.; Grzesiek, S. *J. Biomol. NMR* **1997**, *10*, 403−408.

(15) Wang, A. C.; Bax, A. *J. Am. Chem. Soc.* **1995**, *117*, 1810−1813.

10.1021/ja001798p CCC: $19.00
Published on Web 10/07/2000

The ab initio prediction of vicinal *J*-coupling constants and of the associated Karplus parameters by quantum chemical methods has been for decades a major challenge. In the past, general features, such as the locations of minima and maxima of Karplus curves, have been well reproduced, while the magnitudes of the couplings could substantially deviate from experimentally extracted curves.[17,18] Only recently the situation has started to change, mainly due to progress in density functional theory methodology[19] and the increase in available computer power. As a consequence, quantitative computation of vicinal couplings and other useful *J* couplings, including trans-hydrogen bond couplings as well as one- and two-bond couplings, has been achieved.[20−24]

The quantitative prediction of Karplus curves by using quantum-chemical methods is of interest for both theoreticians and experimentalists for a number of reasons. First, the empirically derived Karplus curves neglect structural differences between the crystalline and solution structures, which can make it difficult to transfer them from one system to another. Second, differences between experimental and theoretically predicted ^3J couplings can provide qualitative and quantitative information on motional fluctuations of torsion angles taking place on a wide range of time scales (fs to ms) that otherwise are difficult to monitor by NMR experiments. Third, experimental *J* couplings extracted by different NMR pulse sequence schemes sometimes exhibit systematic differences. The availability of independent information on such couplings may lead to a better understanding of systematic experimental errors. Fourth, *J*-coupling calculations as a function of various degrees of freedom (other than the intervening torsion angle) help to define the validity range of one-dimensional Karplus relationships. Finally, demonstrating that calculations can reliably reproduce experimental parameters of well-studied systems supports the use of calculated Karplus parameters for the interpretation of *J*-coupling data of systems for which empirical Karplus parameters are not (yet) available.

We present here quantum calculations of ^3J couplings of proteins involving the φ and ψ backbone torsion angles by density functional theory (DFT) using the programs deMon[19,25] and Gaussian.[26] The calculations are carried out on a multitude of conformers of two different versions of the alanine dipeptide, Ace-Ala-NMe and Ala-Ala-NH_2, shown in Figure 1. The φ-dependences of six different homo- and heteronuclear ^3J-coupling constants are computed and the corresponding Karplus parameters are extracted and compared to empirical parametrizations reported in the literature. The effects of structure optimizations and of thermal molecular motions of φ-dihedral angles and other degrees of freedom are discussed. By comparing theoretical and experimental *J* couplings of the protein ubiquitin uncertainties and fluctuation amplitudes of φ-dihedral angles are determined.

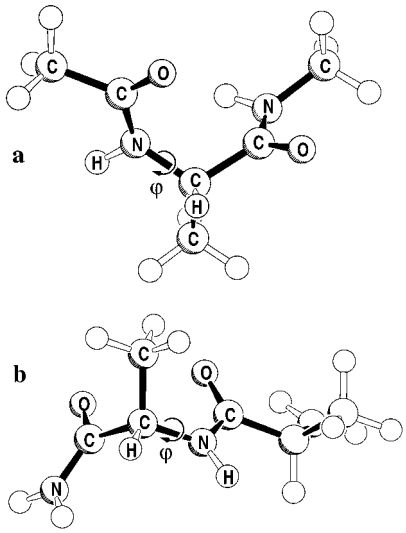

Figure 1. Three-dimensional geometries of the two model systems for which scalar ^3J-coupling constants were calculated using density functional theory (DFT) methods as a function of the φ main-chain torsion angles for differently optimized geometries: (a) Ace-Ala-NMe and (b) Ala-Ala-NH_2.

2. Methods

2.1. Construction of Alanine-Dipeptide Conformers. For the computations carried out on the conformers of Ace-Ala-NMe (Figure 1a) the φ and ψ backbone angles were set to fixed values that are multiples of 30°, and restricted to low-energy regions, as described earlier.[27] The remaining internal degrees of freedom were optimized with either the CHARMM-22 all-atom force field[28] or the Hartree−Fock method with a 6-31G* basis set as implemented in the Gaussian94 program.[26] As expected, there are minor differences in the bond lengths and angles obtained from these optimization procedures, with potentially significant differences in the deviations of the ω-torsion angles from planarity, with the gas-phase Hartree−Fock results showing larger deviations than the empirically derived CHARMM force field. However, as is shown below, these differences have no important consequences for the ^3J-coupling constants.

The conformations for Ala-Ala-NH_2 (Figure 1b) were constructed starting from the X-ray structure of the Ala-Ala dipeptide[29] with local geometries adjusted in accordance to the CHARMM-22 force field and as described previously.[30] The N-terminal NH_3^+ group was replaced

(16) Schmidt, J. M.; Blümel, M.; Löhr, F.; Rüterjans, H. *J. Biomol. NMR* **1999**, *14*, 1−12.
(17) Edison, A. S.; Markley, J. L.; Weinhold, F. *J. Phys. Chem.* **1993**, *97*, 11657−11665. Edison, A. S.; Markley, J. L.; Weinhold, F. *J. Biomol. NMR* **1994**, *4*, 519−542.
(18) Barfield, M. In *Encyclopedia of Nuclear Magnetic Resonance*; Grant, D. M., Harris, R. K., Eds; Wiley: London, 1996; pp 2520−2532.
(19) Malkin, V. G.; Malkina, O. L.; Casida, M. E.; Salahub, D. R. *J. Am. Chem. Soc.* **1994**, *116*, 5898−5908.
(20) Dingley, A. J.; Masse, J. E.; Peterson, R. D.; Barfield, M.; Feigon, J.; Grzesiek, S. *J. Am. Chem. Soc.* **1999**, *121*, 6019−6027.
(21) Scheurer, C.; Brüschweiler, R. *J. Am. Chem. Soc.* **1999**, *121*, 8661−8662.
(22) Cornilescu, G.; Case, D. A.; Bax, A. *J. Am. Chem. Soc.* **2000**, *122*, 2168−2171.
(23) Podlasek, C. A.; Stripe, W. A.; Carmichael, I.; Shang, M.; Basu, B.; Serianni, A. S. *J. Am. Chem. Soc.* **1996**, *118*, 1413−1425. Cloran, F.; Carmichael, I.; Serianni, A. S. *J. Phys. Chem. A* **1999**, *103*, 3783−3795.
(24) Case, D. A. *Curr. Opin. Struct. Biol.* **2000**, *10*, 197−203.
(25) St-Amant, A.; Salahub, D. R. *Chem. Phys. Lett.* **1990**, *169*, 387−392. Salahub, D. R.; Fournier, R.; Mlynarski, P.; Papai, I.; St-Amant, A.; Ushio, J. In *Density Functional Methods in Chemistry*; Labanowski, A., Andzelm, J., Eds.; Springer: New York, 1991; p 77.
(26) Frisch, M. J.; Trucks, G. W.; Schlegel, H. B.; Gill, P. M. W.; Johnson, B. G.; Robb, J. A.; Cheeseman, J. R.; Keith, T. A.; Petersson, G. A.; Montgomery, J. A.; Raghavachari, K.; Al-Laham, M. A.; Zakrzewski, V. G.; Ortiz, J. V.; Foresman, J. B.; Cioslowski, J.; Stefanov, B. B.; Nanayakkara, A.; Challacombe, M.; Peng, C. Y.; Ayala, P. Y.; Chen, W.; Wong, M. W.; Andres, J. L.; Replogle, E. S.; Gomperts, R.; Martin, R. L.; Fox, D. J.; Binkley, J. S.; Defrees, D. J.; Baker, J.; Stewart, J. P.; Head-Gordon, M.; Gonzalez, C.; Pople, J. A. *Gaussian 94*, revision B.2; Gaussian, Inc.: Pittsburgh, PA, 1995.
(27) Sitkoff, D.; Case, D. A. *J. Am. Chem. Soc.* **1997**, *119*, 12262−12273.
(28) MacKerell, A. D., Jr.; Bashford, D.; Bellott, M.; Dunbrack, R. L., Jr.; Evanseck, J. D.; Field, M. J.; Fischer, S.; Gao, J.; Guo, H.; Ha, S.; Joseph-McCarthy, D.; Kuchnir, L.; Kuczera, K.; Lau, F. T. K.; Mattos, C.; Michnick, S.; Ngo, T.; Nguyen, D. T.; Prodhom, B.; Reiher, W. E., III; Roux, B.; Schlenkrich, M.; Smith, J. C.; Stote, R.; Straub, J.; Watanabe, M.; Wiórkiewicz-Kuczera, J.; Yin, D.; Karplus, M. *J. Phys. Chem. B* **1998**, *102*, 3586−3616.
(29) Fletterick, F.; Tsai, C.; Hughes, R. E. *J. Phys. Chem.* **1971**, *75*, 918−922.
(30) Scheurer, C.; Skrynnikov, N. R.; Lienin, S. F.; Straus, S. K.; Brüschweiler, R.; Ernst, R. R. *J. Am. Chem. Soc.* **1999**, *121*, 4242−4251.

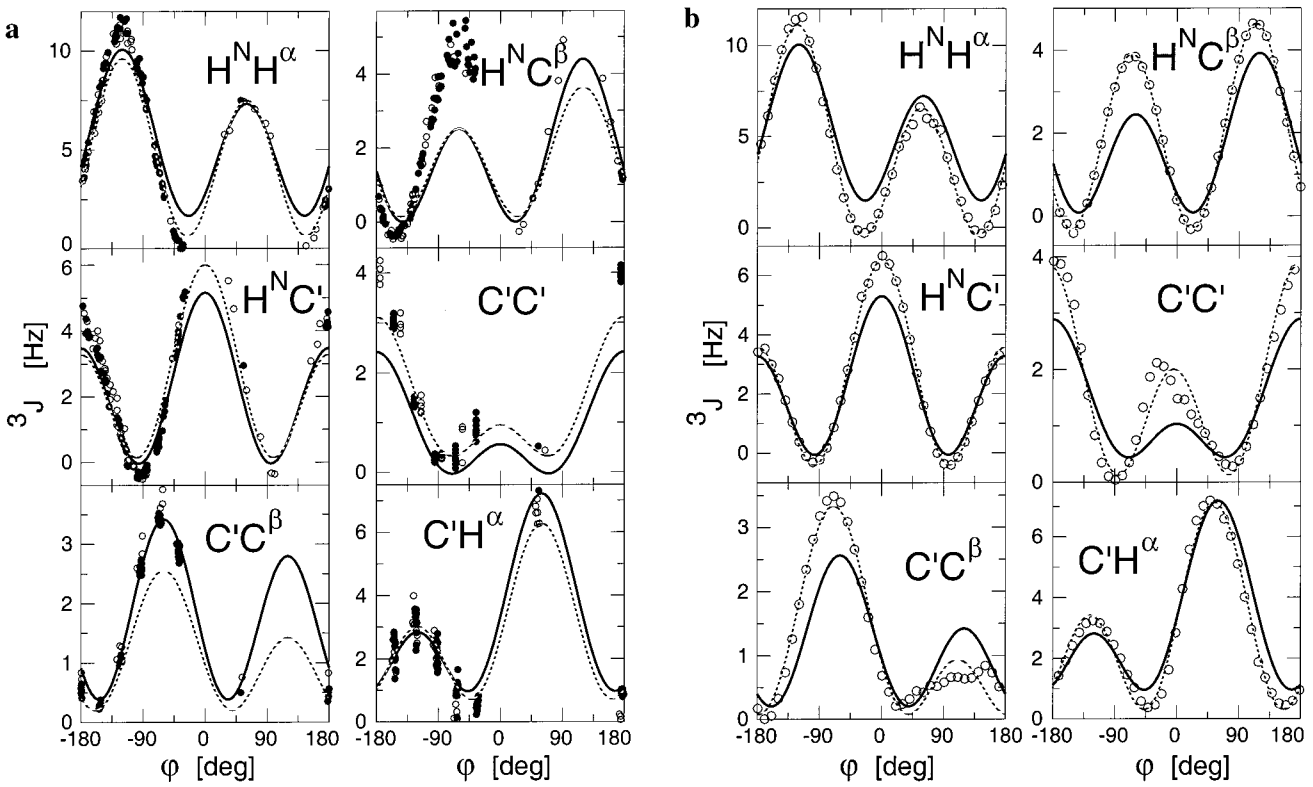

Figure 2. Computed scalar ^3J-coupling constants between spins X and Y for (a) Ace-Ala-NMe and (b) Ala-Ala-NH_2 (see Figure 1) involving the X−N−C^α−Y torsion angle. Spin X belongs either to H^N or C′ and spin Y either to H^α, C^β, or C′. In panel a, the circles give computed ^3J-coupling constants against the angle $\tau - \theta$, where τ is the X−N−C^α−Y torsion angle and the offset angle θ is given in Table 1 ($\tau - \theta$ is approximately the φ-torsion angle): filled circles correspond to CHARMM-optimized structures, while open circles belong to structures optimized by HF/6-31G*. In panel a, empirical Karplus curves based on data from ubiquitin[6−8] are given by solid lines, and the ones based on data from flavodoxin[11] are indicated by dashed lines (plotted against φ). In panel b, the same couplings are given as in panel a for Ala-Ala-NH_2. The open circles correspond to the calculated couplings, the dotted lines indicate the best fit of Karplus curves of the form of eq 1 to the calculated couplings with fit parameters given in Table 1, and the solid lines are the empirical curves for ubiquitin.[6−8]

by a NH_2 group and a NH_2 group was added at the C terminus leading to a charge neutral molecule. The ω angle was kept fixed at the original value of −165° and the φ angle was varied from 0° to 360° in 10° increments.

2.2. *J*-Coupling Calculations by DFT. The quantum chemical calculations of the scalar *J*-coupling constants were performed using the sum-over-states density functional perturbation theory (SOS-DFPT)[19] as implemented in the *deMon NMR* program.[25] All major *J*-coupling contributions were calculated including the Fermi contact (FC) term, the paramagnetic spin−orbit (PSO) term, and the diamagnetic spin−orbit (DSO) term, while the spin−dipolar (SD) term, which is usually only a small fraction of the leading FC term, was neglected. The couplings were calculated using the SOS-DFPT approximation[19] with the Loc.1 energy correction for the denominators and with the molecular orbitals localized by the method of Boys.[32] Full details of the method are given elsewhere.[19] For all calculations the Perdew−Wang exchange functional with the Perdew correlation functional[33] was used, which was previously found to yield *J*-coupling constants that are in good agreement with experimental data.[21,22,31a] Other choices for exchange and correlation functionals can have a significant effect on the *J*-coupling constant as is illustrated in Supporting Information.

Numerical quadrature was carried out on FINE RANDOM angular grids[31c,25] with 64 radial shells. Approximate gauge invariance is obtained using the individual gauge for localized orbitals (IGLO) approach of Kutzelnigg and co-workers.[34] The DFT calculations used the IGLO-III basis set,[34] which contains 11 s-type and 7 p-type Gaussians on first row atoms (contracted to 7s/6p) along with two uncontracted polarization functions. For comparison, some calculations were repeated with a smaller IGLO-II basis, which has 5s and 4p contracted basis functions and a single polarization function on first row atoms. For the Fermi contact term, a finite perturbation approach is used involving a separate calculation for each nucleus. Such a calculation then gives couplings to all other nuclei in the molecule. For the Ace-Ala-NMe dipeptide, each calculation takes about 2.5 h of CPU time on a single processor of a 450 MHz Cray T3E and for the Ala-Ala-NH_2 2 h on a DEC-Alpha (600 MHz) processor and 2.85 h on a Sun SparcUltra 60, respectively. Four such calculations were carried out for each conformer with the perturbation applied at the H^N, H^α, C^β, and C′ positions, respectively.

3. Results and Discussion

3.1. φ Dependence of ^3J-Coupling Constants in the Absence of Motion. There exist six ^3J-coupling constants that involve the φ backbone angle, connecting the carbonyl C′ atom of the previous residue or the H^N atom of the same residue to any of the H^α, C^β, or C′ atoms of the same residue. Traditionally, the most extensively studied coupling has been the proton−proton $^3J(H^N-H^\alpha)$ coupling, but experimental results are now available for two proteins for all the other combinations as well. Figure 2 shows computed results for each of these couplings

(31) (a) Malkin, V. G.; Malkina, O. L.; Salahub, D. R. *Chem. Phys. Lett.* **1994**, *221*, 91−99. (b) Malkina, O. L.; Salahub, D. R.; Malkin, V. G. *J. Chem. Phys.* **1996**, *105*, 8793−8800. (c) Malkin, V. G.; Malkina, O. L.; Salahub, D. R. *Chem. Phys. Lett.* **1996**, *261*, 335−345. (d) Malkin, V. G.; Malkina, O. L.; Casida, M. E.; Salahub, D. R. *J. Am. Chem. Soc.* **1994**, *116*, 5898−5908.

(32) Foster, S.; Boys, S. *Rev. Mod. Phys.* **1960**, *32*, 303−304.

(33) Perdew, J. P.; Wang, Y. *Phys. Rev. B* **1986**, *33*, 8800−8802. Perdew, J. P. *Phys. Rev. B* **1986**, *33*, 8822−8824; Perdew, J. P.; Wang, Y. *Phys. Rev. B* **1992**, *45*, 13244−13249.

(34) Kutzelnigg, W.; Fleischer, U.; Schindler, M. In *NMR: Basic Principles and Progress*; Diehl, P., Fluck, E., Kosfeld, E., Eds.; Springer: Berlin, 1991; Vol. 23, pp 165−262.

Table 1. Coefficients for Karplus Curves of Figure 2 Based on Eq 1

^3J coupling	θ [deg][i]	A [Hz][j]	B [Hz][j]	C [Hz][j]	source	σ [deg][h]
$^3J(H^N-H^\alpha)$	−60	9.44	−1.53	−0.07	DFT 1[a]	
	−64.51	9.14	−2.28	−0.29	DFT 2[b]	
	−60	7.09	−1.42	1.55	ubiquitin[e]	21.7/21.6
	−60	7.90	−1.05	0.65	flavodoxin[f]	17.5/17.5
	−60	9.5	−1.4	0.3	"zero-motion"[c]	
$^3J(H^N-C^\beta)$	60	5.15	0.01	−0.32	DFT 1[a]	
	58.18	4.58	−0.36	−0.31	DFT 2[b]	
	60	3.06	−0.74	0.13	ubiquitin[e]	29.2/25.3
	60	2.90	−0.56	0.18	flavodoxin[f]	30.7/27.1
$^3J(H^N-C')$	180	5.58	−1.06	−0.30	DFT 1[a]	
	172.49	5.34	−1.46	−0.29	DFT 2[b]	
	180	4.29	−1.01	0.00	ubiquitin[e]	20.8/20.1
	180	4.41	−1.36	0.24	flavodoxin[f]	18.9/17.8
$^3J(C'-C')$	0	2.39	−1.25	0.26	DFT 1[a]	
	−2.56	2.71	−0.91	0.21	DFT 2[b]	
	0	1.36	−0.93	0.60	ubiquitin[e]	32.7/32.2
	0	1.51	−1.09	0.52	flavodoxin[f]	27.8/28.6
$^3J(C'-C^\beta)$	−120	2.49	−0.64	0.28	DFT 1[a]	
	−117.55	1.86	−1.20	0.27	DFT 2[b]	
	−120	1.74	−0.57	0.25	ubiquitin[e]	24.3/24.4
	−120	2.72	−0.31	0.39	flavodoxin[f]	0.0/0.0
$^3J(C'-H^\alpha)$	120	4.38	−1.87	0.56	DFT 1[a]	
	118.61	4.77	−1.85	0.49	DFT 2[b]	
	120	3.72	−2.18	1.28	ubiquitin[e]	14.0/18.1
	120	3.76	−1.63	0.89	flavodoxin[f]	16.9/20.3
$^3J(H^\alpha-N)$	60[d]	5.58	−1.06	−0.30	DFT 1[a]	
	60[d]	4.29	−1.01	0.00	ubiquitin[g]	

[a] Parameter fits for Ace-Ala-NMe of Figure 2a. [b] Parameter fits for Ala-Ala-NH_2 of Figure 2b. [c] Extrapolated "zero motion parameters" of ref 40. [d] Dependence with respect to ψ angle (see Figure 6b). [e] Empirical Karplus parameters for ubiquitin from refs 6−8. [f] Empirical Karplus parameters for flavodoxin from ref 16. [g] Empirical Karplus parameters for ubiquitin from ref 15. [h] Average uncertainty in φ determined by comparison of the experimental Karplus relationship with the two DFT (DFT 1/DFT 2) curves using eqs 1 and 2. [i] Offset such that the torsion angle τ between the two coupled spins is $\tau \cong \varphi(\psi) + \theta$ (eq 1). For DFT 1 θ was kept fixed at standard values. [j] Karplus parameters of eq 1.

for Ace-Ala-NMe (Figure 2a) and Ala-Ala-NH_2 (Figure 2b), together with empirical Karplus curves derived from experimental measurements on ubiquitin[6−8] and flavodoxin.[11,16] Figure 2a combines the results for all of the low-energy φ, ψ points in the Ramachandran plot, as described earlier,[27] whereas Figure 2b uses $\psi = -165°$. The close agreement of the two sets of calculations reflects the fact that the ψ-dihedral angle is relatively unimportant for these coupling constants.

Assuming that all couplings follow general Karplus relationships of the form[1]

$$J = A\cos^2(\varphi + \theta) + B\cos(\varphi + \theta) + C \qquad (1)$$

for each type of ^3J coupling the parameters *A*, *B*, *C*, and an offset angle θ were individually extracted by a least-squares fit to the *J* couplings computed using DFT and shown in Figure 2. The values for *A*, *B*, *C*, and θ are given in Table 1. In the original derivation of eq 1 only the Fermi contact term was considered.[1] While the present calculations show that the paramagnetic and diamagnetic spin−orbit terms can have absolute magnitudes exceeding 1 Hz, their sum, however, is generally below 0.1 Hz. Thus, the results presented here predominantly reflect the FC term.

Several interesting features become apparent from Figure 2 and Table 1:

(1) Results arising from CHARMM-optimized structures and from Hartree−Fock 6-31G*-optimized structures (open and solid circles in Figure 2a) lie on essentially the same curves indicating that the couplings do not significantly depend on the method chosen for geometry optimization. Moreover, the results obtained for Ace-Ala-NMe are for most φ regions rather similar to the results obtained for Ala-Ala-NH_2 (see Table 1) indicating that these computations are generally not very sensitive to the size of the selected fragment. Exceptions can be found in Figure 2 concerning mainly the $^3J(H^N-C^\beta)$ coupling around $\varphi = -60°$, where the computed couplings for Ace-Ala-NMe are about 1 Hz larger than those for Ala-Ala-NH_2 and for the $^3J(C'-C')$ coupling around $\varphi = 0°$, where the computed coupling for Ace-Ala-NMe is about 1 Hz smaller than for Ala-Ala-NH_2. For Ala-Ala-NH_2 with the ω angle fixed at −165° pronounced deviations from Karplus-type behavior occur for the $^3J(C'-C')$ curve around $\varphi = 0°$ and for the $^3J(C'-C^\beta)$ curve for $30° < \varphi < 120°$. These are due to close sterical contacts between the two carbonyl oxygens and between the first carbonyl oxygen and C^β, respectively. Both curves exhibit the expected Karplus behavior if ψ is allowed to change during energy minimization relaxing the sterical interaction. Since the changes in ψ that are introduced by this procedure can be rather large, the DFT calculations with fixed $\psi = -165°$ have been chosen as the basis for the Karplus parametrizations.

(2) The quantum-chemically determined *J*-coupling constants generally exhibit a smooth dependence on the intervening torsion angle, as shown in Figure 2. This torsion angle is approximately, but not precisely, related to the conventional backbone dihedral angle φ defined by the atoms $C'-N-C^\alpha-C'$. Particularly for the $^3J(H^N-H^\alpha)$ coupling, this distinction is important: a plot of coupling constant vs φ is less than smooth the one of Figure 2a. Almost all ^3J-coupling constants are predominantly determined by the φ angle. The most noticeable deviation from this behavior is for the $C'-H^\alpha$ coupling (Figure 2a), where conformations with the same value of φ but different values of ψ have a range of couplings with a spread of nearly 2 Hz.

All curves can be rather well parametrized by the general expression of eq 1 with the restrictions mentioned above. The latter indicates that geometric features other than the intervening torsion angle may in some cases significantly contribute to the ^3J coupling. For the other couplings, the spread in computed results for structures with a fixed φ value is less than 0.5 Hz. With the exceptions noted, this means that the conventional interpretation of ^3J couplings in terms of the intervening torsion angle is justified and that the influence of other geometrical parameters is minor. Thus, these computations provide an explicit quantum-chemical foundation for the validity range of Karplus relationships for ^3J couplings between spin pairs connected by the backbone φ angle. The situation is more complicated for ^3J couplings with ψ as the major intervening torsion angle, as discussed in Section 3.5.

(3) The largest discrepancy between the quantum-chemical and the empirical Karplus relationships are found for the $^3J(H^N-C^\beta)$ coupling at φ around −60°, where the calculated couplings are 2−3 Hz larger than the measured ones. This discrepancy is caused in part by motional averaging effects, as discussed in the following section, but interestingly the computed couplings for Ace-Ala-NMe and Ala-Ala-NH_2 do also differ (compare Figure 2a,b). This may indicate that in this range the $^3J(H^N-C^\beta)$ coupling is more susceptible to the size of the fragment and possibly also to the identity of the side chain. For example, replacement of Ala in Ace-Ala-NMe by a serine and use of a larger basis set leads to a reduced coupling constant of about 4 Hz. Further studies on the side-chain dependence of the $^3J(H^N-C^\beta)$ coupling will be useful.

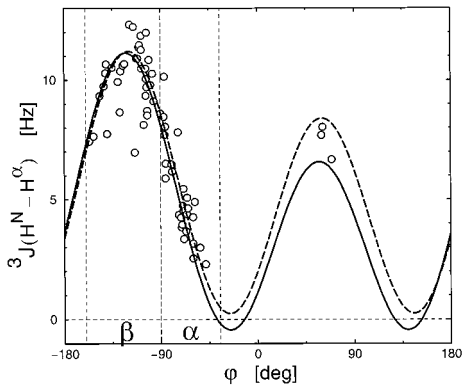

Figure 3. DFT results (open circles) of the $^3J(H^N-H^\alpha)$ coupling for Ala-Ala-NH_2 fragments with geometries taken from atom coordinates along the backbone of ubiquitin of a molecular dynamics snapshot after 1 ns. Superimposed are computed Karplus curves of Table 1 for Ala-Ala-NH_2 (DFT 2, solid line) and the "zero motion" curve[40] (dashed line).

3.2. Instantaneous ^3J-Coupling Constants in the Presence of Motion. The quantum calculations described in the previous section were performed on geometry optimized structures. In reality, however, observed scalar ^3J couplings correspond to the time- and ensemble-average over structures that exhibit local fluctuations (bending, stretching, etc.) and fluctuations of the φ-torsion angle itself. To assess these two effects, DFT calculations were performed on snapshots taken from a molecular dynamics (MD) simulation of ubiquitin at room temperature in explicit water solvent using CHARMM 24[28,35] (for more details on the simulation see ref 36).

First, instantaneous $^3J(H^N-H^\alpha)$ couplings were calculated from a single snapshot after 1 ns by converting the Cartesian coordinates of the backbone and C^β atoms of pairs of adjacent amino acids from the snapshot to Ala-Ala-NH_2 dipeptide structures. Effects of the protein environment were included in terms of partial point charges using the charge field perturbation approach.[37] In Figure 3, the resulting couplings are plotted against the instantaneous φ torsion angles. The points are scattered around the Karplus curves given in Table 1 indicating that for the $^3J(H^N-H^\alpha)$ coupling and for these ranges of torsion angles thermal motions causing non-ideal local geometries of degrees of freedom other than the φ angle do not introduce a significant systematic bias with respect to the underlying Karplus curve.

Using a procedure analogous to the one developed for the assessment of local fluctuations of chemical shielding anisotropies in proteins,[30] the time-evolution of ^3J couplings can be studied in some detail (Figure 4). All six ^3J couplings involving the φ angle were computed by DFT applied to Ala-Ala-NH_2 fragments with geometries taken from ubiquitin snapshots for (a) Lys 29−Ile 30 (α-helical region) and (b) Arg 42−Leu 43 (β strand region) and plotted against the respective instantaneous φ torsion angle (Figure 4). A total of 50 snaphots of the MD trajectory were selected starting at 500 ps with a time increment of 16 ps. The points generally scatter uniformly around the computed Karplus curves of Table 1 introducing little to no bias with respect to the theoretical curves (solid lines). An exception is the β-region of the $^3J(C'-C')$ coupling where non-ideal geometries lead to a clear increase of this coupling. The figure demonstrates that for fixed φ angle, the thermal averages of these ^3J couplings are quite insensitive to the details of local atomic fluctuations. Thus, ^3J-coupling averaging over φ-angle distributions can be carried out independently of the averaging over other degrees of freedom.

3.3. Averaged ^3J-Coupling Constants in the Presence of Motion. At the local maxima of the Karplus curves of Figure 2, the computational results are generally somewhat higher than the empirical curves. This is an expected result, which is related to the nature of J-coupling averaging due to local torsional fluctuations.[38−40] Since each quantum-chemical computation assumes a fixed φ-torsion angle, the resulting J-coupling dependences correspond to static Karplus curves, that is, curves in the absence of molecular motion. On the other hand, experimental J couplings measured at room temperature invariably contain some amount of averaging of the torsion angles about the mean positions. In particular, near the maxima of the Karplus relationship, such averaging will lower observed couplings compared to an idealized static case. The effect of Gaussian fluctuations of the backbone torsion angle φ with a variance σ^2 on the ^3J-coupling constant can be analytically described: the averaged ^3J-coupling constant still follows eq 1 as a function of the average torsional angle $\bar{\varphi}$ (instead of φ), but with modified coefficients A', B', C' depending on the original coefficients A, B, C, and the variance σ^2:

$$A' = A\exp(-2\sigma^2), \quad B' = B\exp(-\sigma^2/2), \quad C' = C + A(1-\exp(-2\sigma^2))/2 \quad (2)$$

[40] where σ has units of radians. On the basis of MD results,[36] this motional model is expected to be realistic for most parts of the protein backbone of ubiquitin. For the J-coupling analysis of mobile side chains additional averaging over different rotamers would be required.

Uncertainties in the averaged φ angles can lead to a similar effect. If an X-ray structure is taken for reference such uncertainties can arise due to discrepancies between the X-ray and the solution structure. On the other hand, if a NMR structure is taken as a reference, experimental errors of the backbone φ dihedral angles can cause the same type of effect. If motional effects are independent of structural uncertainties and if both are assumed to be Gaussian distributed, the total σ^2 of eq 2 can be decomposed into

$$\sigma_{tot}^2 = \sigma_{dyn}^2 + \sigma_{struct}^2 \quad (3)$$

where σ_{dyn} denotes the standard deviation of φ dynamics averaged over the whole protein backbone and σ_{struct} denotes the average error in φ.

In ref 40 a large set of empirically parametrized $^3J(H^N-H^\alpha)$ Karplus curves reported in the literature for different proteins was explained by differential angular averaging and an extrapolated "zero-motion" Karplus curve was determined. As can be seen in Table 1 and Figure 3, the static Karplus curves for $^3J(H^N-H^\alpha)$ found here by quantum-chemical computations closely match that extrapolation, particularly for negative φ angles, supporting both the basic idea of motional averaging and the quantitative accuracy of the present calculations.

(35) Brooks, R. B.; Bruccoleri, R. E.; Olafson, B. D.; States, D. J.; Swaminathan, S.; Karplus, M. *J. Comput. Chem.* **1983**, *4*, 187−217.
(36) Lienin, S. F.; Bremi, T.; Brutscher, B.; Brüschweiler, R.; Ernst, R. R. *J. Am. Chem. Soc.* **1998**, *120*, 9870−9879.
(37) deDios, A. C.; Pearson, J. G.; Oldfield, E. *Science* **1993**, *260*, 1491−1496.
(38) Hoch, J. C.; Dobson, C. M.; Karplus, M. *Biochemistry* **1985**, *24*, 3831.
(39) Karimi-Nejad, Y.; Schmidt, J. M.; Rüterjans, H.; Schwalbe, H.; Griesinger, C. *Biochemistry* **1994**, *33*, 5481.
(40) Brüschweiler, R.; Case, D. A. *J. Am. Chem. Soc.* **1994**, *116*, 11199−11200.

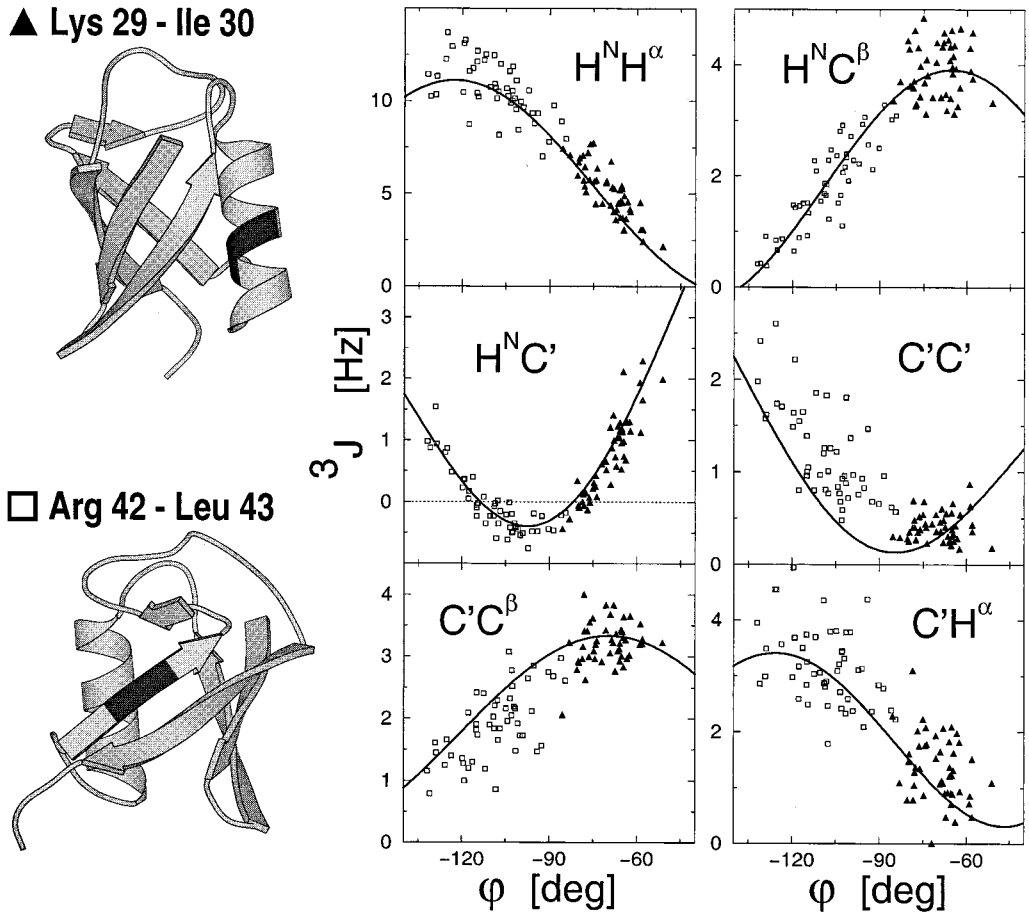

Figure 4. Time dependence of scalar ^3J couplings determined by DFT calculations applied to Ala-Ala-NH_2 fragments with geometries taken from ubiquitin snapshots for Lys 29−Ile 30 (filled triangles), located in the α helix, and Arg 42−Leu 43 (open squares) located in a β strand. A total of 50 snaphots of the MD trajectory were selected starting at 500 ps with a time increment of 16 ps. The superimposed curves correspond to the "DFT 2" Karplus parameters of Table 1.

Standard deviations σ were determined by comparison between the experimentally derived Karplus relationships of ubiquitin[6−8] with the ones of the present DFT calculations. The results are given in Table 1. For ubiquitin the largest σ values are found for the $^3J(C'-C')$ coupling (32.7°) and the smallest one for $^3J(C'-H^\alpha)$ (14°−18°), while for flavodoxin σ varies between 30.7° for $^3J(H^N-C^\beta)$ and 0° for $^3J(C'-C^\beta)$. $\sigma = 0°$ is the result of the notably large dynamic range of the experimental $^3J(C'-C^\beta)$ couplings of flavodoxin exceeding the ones of both DFT calculations as well as the experimental range for ubiquitin. For ubiquitin the average σ value is 23.7° ± 5° and for flavodoxin 22.3° ± 5°. These values are protein specific, reflecting both the protein's backbone φ-angle dynamics and the accuracy with which its backbone structure is known.

3.4. φ Fluctuations of Individual Amino Acids of Ubiquitin. To discriminate between dynamic and structural contributions, σ_{dyn} and $\bar{\varphi}$ were determined for individual φ angles of ubiquitin by using the following procedure: starting from the DFT Karplus parameters for the six ^3J couplings (DFT 2 values of Table 1) σ_{dyn} and $\bar{\varphi}$ were adjusted in eqs 1 and 2 until the experimental scalar ^3J couplings of ubiquitin[6−8] were best reproduced by minimizing the χ^2 function in the least-squares sense

$$\chi^2 = \sum_{k=1}^{4-6} ({}^3J_{k,\mathrm{DFT}}(\bar{\varphi}, \sigma^2_{\mathrm{dyn}}) - {}^3J_{k,\mathrm{exp}})^2 \qquad (4)$$

where k numbers the available ^3J_k couplings involving φ. φ angles for which less than four experimental ^3J couplings are available were not included in the analysis. These are φ_{10}, φ_{19}, φ_{24}, φ_{35}, φ_{37}, φ_{38}, φ_{47}, φ_{53}, φ_{72}, φ_{75}, and φ_{76}. For the remaining 64 residues the minimal χ^2 varies between 0.25 and 1.53 Hz^2 with an average of 0.68 ± 0.32 Hz^2. A χ^2 of 0.68 Hz^2 typically corresponds to an average difference between experimental and back-calculated J couplings of about 0.33 Hz. The average value of σ_{dyn} for these residues is 24.0° with a standard deviation of ±8°. The optimized $\bar{\varphi}$ values can be compared with the φ angles of the X-ray structure[41]

$$\sigma_{\mathrm{struct}} = \left(\frac{1}{64}\sum_{j=1}^{64}(\bar{\varphi}_j - \varphi_{\mathrm{X-ray},j})^2\right)^{1/2} \qquad (5)$$

yielding a value of $\sigma_{struct} = 8.0°$. Thus, $\sigma_{eff} = (\sigma^2_{dyn} + \sigma^2_{struct})^{1/2} = 25.3°$, which is in good agreement with the global analysis described in the previous section ($\sigma_{eff} = 23.7°$). For ubiquitin $\sigma_{dyn}/\sigma_{struct} \cong 3$: thus the differences between the backbone φ angles in the crystalline and the liquid state of ubiquitin are on average a factor of 3 smaller than the fluctuation amplitudes of the φ angles due to thermal motion.

For residues Ala 46, Asn 60, and Glu 64, which are the only residues with positive φ angles, the fitted σ_{dyn} values are notably low (below 1°) with $|\bar{\varphi} - \varphi_{X-ray}| < 4°$ and with χ^2 errors of 0.28, 0.95, and 0.46, respectively. This may indicate that these

(41) Alexeev, F.; Bury, S. M.; Turner, M. A.; Ogunjobi, O. M.; Muir, T. W.; Ramage, R.; Sawyer, L. *Biochem. J.* **1994**, *299*, 159−163 (PDB file 1UBI).

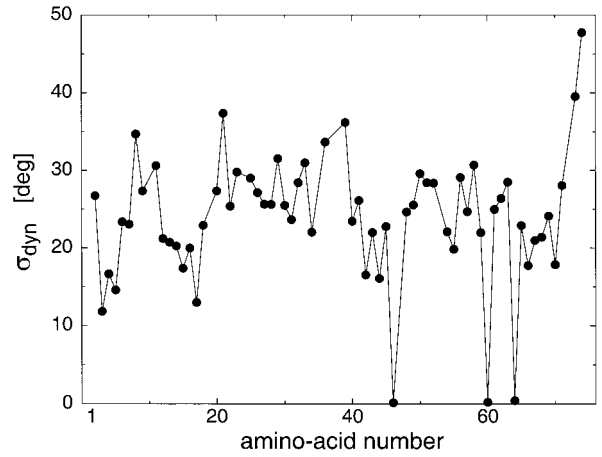

Figure 5. Fluctuation amplitudes σ_{dyn} of backbone φ-torsion angles of ubiquitin determined by a least-squares fit of $\bar{\varphi}$ and σ_{dyn} using eqs 1, 2, 4, and DFT Karplus curves of Table 1 to experimental ^3J-coupling constants involving the φ angles.[6−8]

φ angles are motionally quite constrained or that the DFT Karplus parameters for positive φ angles may require further refinement. The other fitted σ_{dyn} values, which are displayed in Figure 5, vary between 11.8° for φ_3 and 47.6° for φ_{74}. Since ^3J couplings reflect motions on a larger range of different time scales, it is not unexpected that the σ_{dyn} values are larger than what was previously found based on ^{15}N and ^{13}C′ relaxation data of ubiquitin.[36] Since the latter probe only motions on femtosecond to nanosecond time scales, torsion angle fluctuation amplitudes derived from scalar couplings provide an upper limit for motional amplitudes extracted from relaxation parameters. Interestingly, the central α helix (residues 23−34) shows consistently high σ_{dyn} values with an average of 27.2° ± 3°, which is significantly higher than what has been deduced from relaxation experiments and MD simulations.[40,36] This result suggests that on time scales slower than what can currently be monitored by heteronuclear relaxation and MD simulation techniques, that is, slower than about 10^{-8} s, the helix backbone experiences additional local motions. In contrast, the N-terminal β sheet with the exception of the mobile loop shows fluctuations around 20°, which is closer to what one expects from nuclear spin relaxation and MD.

3.5. ψ Dependence of ^3J-Coupling Constants. The dominant dependence of a ^3J coupling on a single torsion angle does not necessarily apply for other types of backbone ^3J couplings. For example, the characterization of the ψ backbone angle by ^3J couplings, such as $^3J(H^\alpha-N)$ and $^3J(N-N)$, is more complex. As an illustration, results for the $^3J(N-N)$ coupling as a function of ψ for two values of the φ backbone torsion angle ($\varphi = -60°$ and $\varphi = -120°$) are plotted in Figure 6a. These calculations are based on the HF/6-31G*-optimized structures of Ace-Ala-NMe. Similar to Figure 2a, there is a spread of about 0.3 Hz among structures optimized by different methods, or with different values of φ. This uncertainty, which is a significant fraction of the J-coupling magnitude ranging from −0.8 to +0.6 Hz, suggests that the $^3J(N-N)$ coupling does not obey the usual one-dimensional Karplus-type relationship, but rather needs to be parametrized in a two- or even higher dimensional parameter space. On a qualitative level it appears that negative couplings are associated with negative values of ψ, that is, primarily with helical regions, whereas positive couplings correlate with positive ψ values found in β sheets and turns.

Similar effects arise for $^3J(H^\alpha-N)$ couplings as shown in Figure 6b. As for $^3J(N-N)$, it is clear that geometric parameters other than the primary intervening ψ torsion angle are important in determining the coupling: structures with the same ψ angle but different values of φ have computed couplings that vary by as much as 0.7 Hz, which is a substantial fraction of the 2 Hz range (from −1.5 to +0.5 Hz) of the entire data set. As deduced experimentally[5,13,15] structures in the helical region (near $\psi = -60°$) show negative couplings of −1.0 to −1.5 Hz, whereas conformers in the β region of conformational space will be closer to zero or slightly positive.

4. Conclusions

Increasingly accurate experimental and theoretical scalar couplings offer interesting new possibilities for the assessment of uncertainties and molecular motion of backbone φ torsion angles and other dihedral angles. Since the average J coupling is sensitive to the amount of motion but is largely insensitive to the motional time scale (coalescence effects excluded), information on the effect of torsion angle dynamics ranging from femtosecond to millisecond time scales can be gained that is otherwise difficult to obtain. Such information is complementary

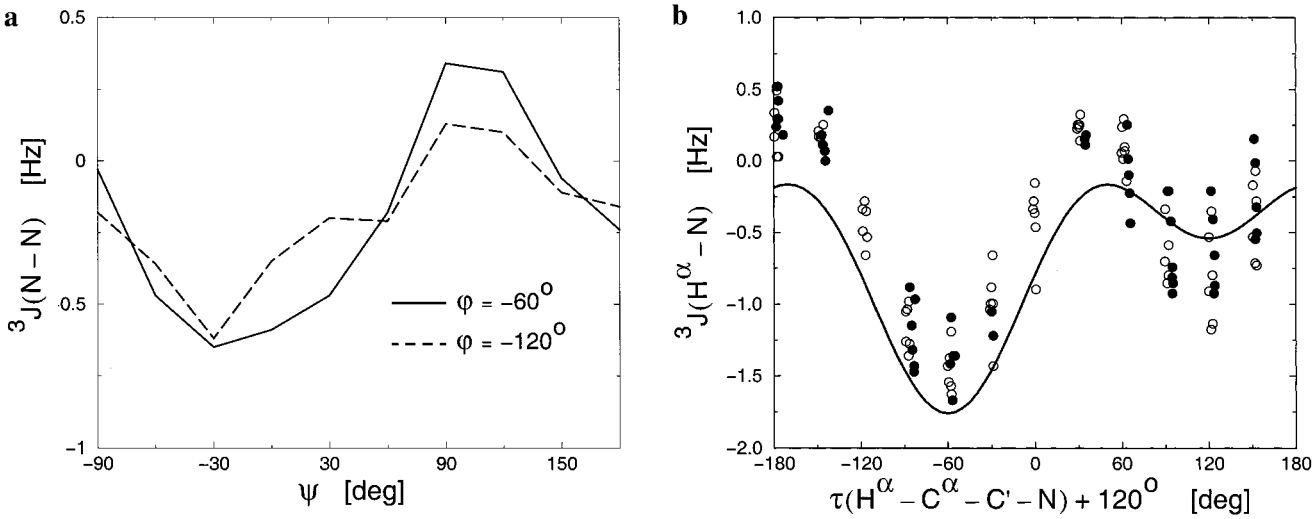

Figure 6. ψ-Torsion angle dependence of $^3J(N-N)$ and $^3J(H^\alpha-N)$ couplings of Ace-Ala-NMe. (a) $^3J(N-N)$ plotted for two different φ torsion angles, $\varphi = -60°$ (solid line) and $\varphi = -120°$ (dashed line), against the ψ-backbone torsion angle for the CHARMM optimized structures. (b) $^3J(H^\alpha-N)$ couplings computed for CHARMM optimized structures (filled circles) and HF6-31G* optimized structures (open circles) as a function of the $H^\alpha-C^\alpha-C'-N$ torsion angle ($\tau \approx \psi - 120°$). The solid line is the empirical Karplus curve proposed by Wang and Bax.[15]

to motional information extracted from dipolar and CSA spin relaxation experiments, which sensitively probe picosecond to nanosecond motions.[36]

Empirically derived Karplus curves for ^3J couplings along the backbone of proteins with known structure tend to show significant variations,[40] which hampers their transferability to new proteins. The emergence of quantum-chemical methods as a quantitative tool for the computation of scalar *J* couplings leads to a detailed understanding of such effects and of possible limitations of one-dimensional Karplus-type relationships. Discrepancies between sets of calculated and measured *J*-coupling constants can be used to reconstruct torsion angle fluctuations about their average values covering time scales that are much slower than the ones accessible by dipolar and CSA nuclear spin relaxation. Thus, the combination of experimental data with the MD/DFT approach is capable to further enhance the information content of *J* couplings as unique probes of the structure and dynamics of biomolecules.

Acknowledgment. This work was supported by NIH Grant GM45811 (to D.A.C.) and by NSF Grant MCB-9904875 (to R.B.). The *deMon* density functional programs were kindly supplied by Professor D. R. Salahub, Professor V. G. Malkin, and Dr. O. L. Malkina.

Supporting Information Available: Vicinal *J*-coupling calculations using a variety of different functionals (PDF). This material is available free of charge via the Internet at http://pubs.acs.org.

JA001798P